

# Magnetic field-induced mixing of hyperfine states of Cs $6^2P_{3/2}$ level observed with a sub-micron vapor cell

Aram Papoyan, David Sarkisyan

*Institute for Physical Research, NAS of Armenia, Ashtarak-2, 378410 Armenia*

Kaspars Blush, Marcis Auzinsh

*Department of Physics, University of Latvia, 19 Rainis blvd., Riga*

*LV-1586, Latvia*

Daniel Bloch, Martial Ducloy

*Labaratoire de Physique des Lasers, UMR 7538 du CNRS, Institut Galilee,*

*Université Paris-Nord, 93430 Villetaneuse, France*

*(version 3.0)*

## Abstract

The fluorescence spectra of a sub-micron atomic cesium vapor layer observable under resonant excitation on D2 line have been studied in the presence of an external magnetic field. Substantial changes in amplitudes and frequency positions of the individual (resolved) hyperfine transitions have been recorded in moderate magnetic fields (up to  $\sim 50$  Gauss). These features are caused by mixing of the hyperfine states of the upper level resulting from comparable values of the hyperfine splitting of the  $6^2P_{3/2}$  manifold and Larmor frequencies of the magnetic sublevels. The results of simulation show a good agreement with the experimental spectra. Possible application of the results for high spatial resolution magnetometry is discussed. *PACS number(s): ???*

## I. INTRODUCTION

It is well known that application of an external magnetic field modifies absorptive and dispersive properties of an atomic system. As magnetic field strength starts to increase from zero value, the degeneracy of atomic states lifts, and magnetic sublevels diverge. The linear shift of these sublevels takes place until the  $B$ - field values for which the Zeeman splitting becomes comparable to the hyperfine splitting of atomic levels. In this regime, the wave functions of the hyperfine manifold begin to mix with each other. This mixing results in dual consequences. First, the shift of magnetic sublevels is no more linear on  $B$ - field (and of different behavior for different individual sublevels). Second, probabilities of the optical transitions between the magnetic sublevels of the lower and upper atomic states differ from unperturbed values [1]. For the first excited levels of Rb and Cs, the atoms of particular interest for spectroscopic studies, the linear Zeeman regime ceases at  $B < 100$  Gauss. Thus, crossing of magnetic sublevels for  $5^2P_{3/2}$  manifold of  $^{85}\text{Rb}$  occurs at  $B \approx 4$  Gauss [2]. Since magnetic splitting in these conditions is incomparably smaller than Doppler broadening, direct observation of hyperfine sublevels mixing effects in absorption and fluorescence spectra for vapor media becomes rather complicated. That is why the studies were done either for higher magnetic fields [1], or by non-direct methods like selective reflection spectroscopy [3,4] at lower magnetic fields. Also the alignment to orientation conversion observation can be used as a very sensitive tool to study level mixing due to different perturbations (see [5,6] and references therein) including atoms with hyperfine structure in a magnetic field [2].

Development of extremely thin vapor cells (ETC) of a sub-micron thickness [7] has opened new possibilities for high resolution spectroscopy of vapor (gaseous) media, allowing one to directly record sub-Doppler lines in the fluorescence and transmission spectra. In particular, as is shown in [7], all the six hyperfine transitions of the Cs atomic D2 line are completely resolved in the fluorescence spectrum (Fig.1 shows hyperfine levels and transitions relevant for this line). Moreover, it should be noted that the amplitude ratios for the individual hyperfine transitions are practically independent of exciting radiation intensity.

The latter indicates that the optical depopulation pumping on the non-cycling transitions  $F_g = 3, 4 \rightarrow F_e = 3, 4$  doesn't establish even at the laser intensities of  $I_L \sim 50 \text{ mW/cm}^2$  for the sub-micron vapor column length. This property is of importance for quantitative spectroscopic and magneto-optical measurements.

Absorption and emission processes in the sub-micron-thick dilute vapor layer are strongly affected by anisotropic geometrical factor. For the atoms flying with mean thermal velocity normally to the window surface (that is "Doppler-sensitive" direction), the wall-to-wall flight time is only  $\sim 1 \text{ ns}$ , i.e., much less than inverse natural width of the optical transition. Fast atoms simply do not have time to absorb, and especially to emit before getting de-excited on the dielectric surface. As a result, the contribution of slow longitudinal velocity atoms in the spectra becomes predominant, giving rise to Dicke-type sub-Doppler features. And since the use of the ETC allows to substantially diminish the Doppler broadening of spectral lines, the influence of the magnetic field on individual hyperfine components can be revealed at weaker magnetic fields as compared with well-known experiments on upper-state level mixing and crossing in Doppler-broadened gases. Hence, the gradual **I** – **J** decoupling as a magnetic field increases can be studied in detail.

Up to now, magnetic field-induced effects in thin cells of radiation wavelength-scale thickness have been studied only theoretically [8]. In this study, peculiarities of Faraday rotation and magnetic circular dichroism have been considered.

In present work, we have studied the influence of magnetic field on fluorescence spectra of a sub-micron Cs vapor layer. The choice of fluorescence rather than absorption studies was justified by better spectral resolution of the individual hyperfine lines [7].

## II. EXPERIMENTAL

Schematic drawing of the measurement configuration is shown in Fig.2. The radiation beam ( $\varnothing 3 \text{ mm}$ ) of the  $\lambda = 852 \text{ nm}$ , 20 MHz-linewidth single-frequency *cw* laser diode was directed at normal incidence onto the ETC of  $\sim 300 \text{ nm}$  thickness with the side arm

containing cesium. The cell was placed in the 3 pairs of mutually perpendicular Helmholtz coils providing possibility to cancel the ambient magnetic field and to apply homogeneous magnetic field in arbitrary direction. The laser frequency was linearly scanned in the region of  $\nu_3$  or  $\nu_4$  transitions of Cs atom (Fig.1). A Glan-Thomson prism was used to purify original (linear) radiation polarization of the laser diode; to produce a circular polarization, a  $\lambda/4$  plate was utilized. A photodiode followed by an operation amplifier was placed at  $90^\circ$  to the laser propagation direction to detect the fluorescence signal emerging through one of two side openings of the cell oven. The photodiode collected emission within  $\sim 0.1$  srad solid angle.

Intensity of the fluorescence emission (with no spectral and polarization analysis) from the vapor layer excited by linearly and circularly polarized radiation was recorded versus the laser radiation frequency, for various directions and magnitudes of the external magnetic field. For the case of longitudinal magnetic field ( $\mathbf{B}/\mathbf{k}$ ), notations of right- and left-handed circular (elementary) polarizations are  $\sigma^+$  and  $\sigma^-$ , respectively. As one could expect, switching from  $\sigma^+(\sigma^-)$  to  $\sigma^-(\sigma^+)$  by adjusting the  $\lambda/4$  plate keeping invariable direction of the magnetic field  $+B$  in this case was completely identical to switching magnetic field from  $+B$  to  $-B$  keeping invariable polarization helicity  $\sigma^+(\sigma^-)$ . Indeed, the recorded signals in these two cases were the same, and for technical convenience, the second option has been exploited for the regular measurements. Over 80 experimental spectra have been recorded with the  $B$ -field strength ranged from 0 to 55 Gauss (the maximum field produced by the set of Helmholtz coils we have used), with the step of 11 Gauss. In fact, some influence of the magnetic field is clearly observable already at  $B \sim 10$  Gauss, but to avoid cumbersome graphical presentation, we will restrict ourselves by the limiting cases of  $B = 0$  and  $B = 55$  Gauss (in the latter case the effect of the  $B$ -field is the most visible).

Scatter circles in Figs.3-5 show the examples of the recorded fluorescence spectra. The orientations of the  $B$ -field are:  $B = B_z$  (Fig.3),  $B = B_x$  (Fig.4), and  $B = B_y$  (Fig.5). Figs.3-5,*a* represent the results for  $\nu_3$  transitions ( $F_g = 3 \rightarrow F_e = 2, 3, 4$ ), and Figs.3-5,*b*

show the results for  $\nu_4$  transitions ( $F_g = 4 \rightarrow F_e = 3, 4, 5$ )<sup>1</sup>. In all the figures, the upper row of graphs are  $B = 0$  spectra, and the lower row graphs are  $B = 55$  Gauss spectra. Notations for every column indicate the applied laser radiation polarization and  $B$ -field orientation. In fact, the same  $B = 0$  spectra with linear and circular laser radiation polarization are presented in the upper rows of all these figures, and they are repeated just to stress the modifications induced by a magnetic field in every particular case (for visual comparison). The vertical (intensity) scale is the same for all the graphs; the horizontal (frequency) scale is 200 MHz/div, the frequency rises rightwards. Saturated absorption signal from an auxiliary 1.5 cm-long Cs cell has been used as a frequency marker (reference). The temperature of the side arm reservoir of the cell (the latter defined the saturated vapor pressure) was kept at  $T_r = 105$  °C throughout the measurements. Corresponding number density of Cs atoms is  $N_{Cs} = 2 \times 10^{13}$  cm<sup>-3</sup>, and the width of collisional (homogeneous) broadening of the spectral lines is  $\approx 1.8$  MHz, i.e. nearly 3 times smaller as compared with the natural line width. The Doppler (inhomogeneous) line width at this temperature regime is  $\approx 440$  MHz.

In agreement with nearly linear intensity dependence of the fluorescence reported in [7], the shape of fluorescence spectrum does not noticeably depend on laser radiation intensity, at least in the range of  $I_L = 1 - 50$  mW/cm<sup>2</sup>. All the spectra presented in graphs were recorded with  $I_L = 40$  mW/cm<sup>2</sup>. For  $I_L < 1$  mW/cm<sup>2</sup>, the fluorescence signal is too weak to be recorded. On the other hand, focussing of the laser beam is required to get higher laser intensities  $I_L > 50$  mW/cm<sup>2</sup>, but in this case the interaction time (time of flight) changes simultaneously; focussing also decreases the number of atoms contributing to the fluorescence signal. The spectra remain invariable under reversal of direction of the laser

---

<sup>1</sup>These notations are valid for  $B = 0$ . As **I** – **J** decoupling starts to develop in the  $B$ -field, the levels that initially are not accessible due to dipole transition selection rules, start to contribute to optical transitions. Hence, it is more correct to write  $F_g = 3 \rightarrow F_e = 2, 3, 4, (5)$  for  $\nu_3$  and  $F_g = 4 \rightarrow F_e = (2), 3, 4, 5$  for  $\nu_4$ .

frequency scanning. Substantial difference in spectra for right-handed ( $\sigma^+$ ) and left-handed ( $\sigma^-$ ) circular polarizations of the laser radiation is observed only for longitudinal direction of the  $B$ -field ( $B = B_z$ , Fig.3). For the case of transverse magnetic field (Figs.4,5), the helicity of light is of no relevance, and the corresponding spectra are identical. Moreover, the spectra with circularly-polarized excitation for  $B = B_x$  (Fig.4) and  $B = B_y$  (Fig.5) are practically identical. These observations are well understandable from symmetry reasons.

As we can see from Figs.3-5, the individual magnetic subtransitions  $m_{F_g} \rightarrow m_{F_e}$  of the same hyperfine transition  $F_g \rightarrow F_e$  are not resolved in the conditions of present experiment. Indeed, in the case of complete resolution, one could expect to see 18 magnetic transitions for the  $\nu_3$  line and 24 magnetic transitions for the  $\nu_4$  line for each of elementary polarizations:  $\pi$  (linear,  $\mathbf{B} // \mathbf{E}$ ),  $\sigma^+$  and  $\sigma^-$  (circular,  $\mathbf{B} // \mathbf{k}$ ), and up to 88 magnetic transitions for more complex  $B$ -field orientation cases. The results of experiment can be rather interpreted as  $B$ -field orientation- and magnitude-dependent frequency shift and variation of amplitude of the  $F_g \rightarrow F_e$  hyperfine transitions.

We would like to draw special attention to the results depicted in 3, with dramatic difference between the fluorescence spectra for the  $\sigma^+$  and  $\sigma^-$  polarizations. This non-intuitive behavior reflects magnetic circular dichroism of the Cs atoms (i.e., different absorption coefficients for  $\sigma^+$  and  $\sigma^-$  light in the magnetic field). The most surprising result is that the  $F_g = 3 \rightarrow F_e = 4$  (Fig.3a,  $\sigma^-$  polarization) and  $F_g = 4 \rightarrow F_e = 3$  (Fig.3b,  $\sigma^+$  polarization) are found to be completely suppressed at rather low magnetic fields.

### III. MODEL

We will use the following model to simulate the spectra of the Cs atomic film without a magnetic field and in the magnetic field. First, we will assume that the absorption rate  $\Gamma_p$  is small in comparison with the relaxation rates in ground and excited states, denoted by  $\gamma$  and  $\Gamma$  respectively:  $\Gamma_p < \gamma, \Gamma$ . This assumption is well justified by the observation of fluorescence spectrum independence of the laser intensity. Second, as far as laser line is

rather broad  $\Delta\nu_L \approx 20$  MHz, the laser radiation spectral line that excites atoms is broader than the homogeneous width of the atomic transition. The radiation width of the transition is  $\Gamma_{rad} = 1/(2\pi\tau) \approx 5.2$  MHz, where  $\tau \approx 30.5$  ns is lifetime of Cs in  $6^2P_{3/2}$  state [9].

As we will see further, the conditions for laser excitation of atoms differ substantially when magnetic field is switched off and when it is applied. Let us start with the analysis of excitation of atoms in zero magnetic field.

### A. Zero magnetic field signal

A convenient way to describe excited state atom optical excitation in the broad line approximation is by means of a quantum density matrix  $f_{mm'}$  [10]. We will consider an atom that absorbs laser light polarized in the direction characterized by light electric field vector  $\mathbf{E}_{exc}$ . In the limit of weak absorption, light does not affect atoms in the ground state. All the ground state magnetic sublevels remain equally populated, and no coherences between magnetic sublevels in the ground state are created. In this situation the density matrix of the excited state can be calculated as [11]:

$$f_{mm'} = \frac{\Gamma_p}{\Gamma} \sum_{\mu} \langle F_e m | \hat{\mathbf{E}}_{exc}^* \cdot \hat{\mathbf{d}} | F_g \mu \rangle \langle F_e m' | \hat{\mathbf{E}}_{exc}^* \cdot \hat{\mathbf{d}} | F_g \mu \rangle^*. \quad (1)$$

Transition takes place from the ground state hyperfine level  $F_g$  to the excited state hyperfine level  $F_e$ . Magnetic quantum numbers of the ground state hyperfine level  $F_g$  are denoted by  $\mu$  and magnetic quantum numbers of the excited state hyperfine level  $F_e$  by  $m$  and  $m'$ . Matrix elements of the dot product can be written as [12]

$$\langle F_e m | \hat{\mathbf{E}}^* \cdot \hat{\mathbf{d}} | F_g \mu \rangle = \sum_q (E^q)^* \langle F_e m | d^q | F_g \mu \rangle, \quad (2)$$

where  $E^q$  are cyclic components of light polarization vector. These components, which in general case are complex numbers, are connected with more familiar Cartesian components as follows [10,12]:

$$E^{+1} = -\frac{1}{\sqrt{2}}(E_x - iE_y),$$

$$E^0 = E_z, \quad (3)$$

$$E^{-1} = \frac{1}{\sqrt{2}}(E_x + iE_y).$$

The remaining matrix element  $\langle F_e m | d^q | F_g \mu \rangle$  can be written in an explicit form by means of Wiegner–Eckart theorem [12–14]:

$$\langle F_e m | d^q | F_g \mu \rangle = (-1)^{F_e - m} \begin{pmatrix} F_e & 1 & F_g \\ -m & q & \mu \end{pmatrix} \langle F_e || d || F_g \rangle, \quad (4)$$

where  $\begin{pmatrix} \circ & \circ & \circ \\ \circ & \circ & \circ \end{pmatrix}$  is 3- $j$ m symbol. To calculate still remaining reduced matrix element  $\langle F_e || d || F_g \rangle$ , we will assume the following scheme of formation of hyperfine level angular momentum in ground and excited states:

$$\mathbf{J}_g + \mathbf{I} = \mathbf{F}_g; \quad \mathbf{J}_e + \mathbf{I} = \mathbf{F}_e, \quad (5)$$

where  $\mathbf{J}_g$  and  $\mathbf{J}_e$  denote total electronic angular momentum of an atom in the ground and excited states (including electron spin  $\mathbf{S}$ ), and  $\mathbf{I}$  is the nuclear spin angular momentum. This scheme allows to write the angular part of wave functions of atom in the following form:

$$|F_g\rangle = |(J_g I) F_g\rangle \quad |F_e\rangle = |(J_e I) F_e\rangle,$$

and taking into account that optical transition dipole moment operator acts only upon the electronic angular momentum and does not act upon the nuclear spin angular momentum, we will get the following expression for the remaining reduced matrix element [13,14]:

$$\langle F_e || d || F_g \rangle = (-1)^{J_g + I + F_e + 1} \sqrt{(2F_e + 1)(2F_g + 1)} \begin{Bmatrix} J_g & F_g & I \\ F_e & J_e & 1 \end{Bmatrix} \langle J_e || d || J_g \rangle, \quad (6)$$

where  $\begin{Bmatrix} \circ & \circ & \circ \\ \circ & \circ & \circ \end{Bmatrix}$  is 6j symbol. These last formulas allow to calculate excited state density matrix for different ground and excited state hyperfine levels, rather easy.

Finally, the fluorescence signal for each allowed hyperfine transition from the excited state hyperfine level  $F_e$  to the final hyperfine level  $F_g$  (which may or may not coincide with the level from which absorption took place) can be calculated according to [10]:



$$I = \sum_{mm'\mu} \langle F_e m | \hat{\mathbf{E}}_{obs}^* \hat{\mathbf{d}} | F_g \mu \rangle \langle F_e m' | \hat{\mathbf{E}}_{obs}^* \hat{\mathbf{d}} | F_g \mu \rangle^* f_{m'm}, \quad (7)$$

where  $\mathbf{E}_{obs}$  denotes the polarization of the light to which detector is sensitive. In the case of fluorescence, the general approach to calculation of dipole transition matrix elements entering Eq.(7) is the same as above described method to calculate matrix elements entering expression Eq.(1) for excited state density matrix calculation. If we measure the total intensity of fluorescence, on transitions to both ground state hyperfine levels without discrimination for a specific light polarization, than we simply must take a sum of two fluorescence components with orthogonal polarizations observed in a definite direction and sum of two spectral transitions to the both ground state hyperfine levels with  $F_g = 3$  and  $F_g = 4$ . Such a spectrum simulated for linearly and circularly polarized excitation is given on Fig.6*a,b*. Left and right graphs of the upper rows refer to the absorption of linearly and circularly polarized light, respectively, from the ground state hyperfine level  $F_g = 4$  (case *a*) and  $F_g = 3$  (case *b*). The dashed line represents the sum of three Lorentz type curves centered around the respected hyperfine component frequency. Width of this Lorentz type spectral line is chosen to be equal to 55 MHz. This is a width which gives signals that fit well to experimentally observed ones. For the experimental signal detected in this work, this width includes laser linewidth, absorption linewidth formed by homogeneous linewidth (natural and collisional), and residual Doppler broadening. Of course, when we have a homogeneous linewidth combined with inhomogeneous broadening, the resulting line shape should be a Voigt contour, but just to make model as simple as one could, Lorentz type line shape for each individual peak was chosen to produce Fig.6. This assumes that remaining Doppler broadening is smaller than the homogeneous linewidth. One can see that the relative intensities of spectral components in this simulation differ from relative line strength which can be calculated as [15]

$$W_{F_g \leftarrow F_e} = (2F_e + 1)(2F_g + 1)(2J_e + 1)(2J_g + 1) \times \begin{Bmatrix} J_g & F_g & I \\ F_e & J_e & 1 \end{Bmatrix}^2 \begin{Bmatrix} L_g & J_g & S \\ J_e & L_e & 1 \end{Bmatrix}^2 \quad (8)$$

where  $L_g$  and  $L_e$  are electron orbital momenta for the ground and excited state.

This difference has an obvious explanation. As far as we are using polarized light to excite atoms, the excited state spatial angular momenta distribution of atoms is anisotropic. This anisotropy is different for different types of transitions and depends on quantum numbers  $F_g$  and  $F_e$ . It is especially sensitive to the quantity  $\Delta F = F_g - F_e$ . As a result, radiation emission from the excited state hyperfine levels towards a specific direction in a space differs, among other factors like transition strength, also because of this anisotropy. For more detailed explanation of this effect, see for example [16,17].

## B. Signal with a magnetic field

When an external magnetic field is applied, the Hamilton operator for the atom in a magnetic field can be written as

$$\widehat{H} = \widehat{H}_0 + \widehat{H}_{HFS} - \mu_J \cdot \mathbf{B} - \mu_I \cdot \mathbf{B}. \quad (9)$$

where  $\widehat{H}_0$  is a Hamiltonian operator of unperturbed atom,  $\widehat{H}_{HFS}$  represents hyperfine interaction. The remaining two terms represent interaction of the electronic magnetic moment  $\mu_J$  of atom and the nucleus magnetic moment  $\mu_I$  with the external magnetic field  $\mathbf{B}$ . These magnetic moments are connected with the respective electronic and spin angular moments  $\mathbf{J}$  and  $\mathbf{I}$  of the atom:

$$\mu_J = \frac{g_J \mu_B}{\hbar} \mathbf{J}, \quad \mu_I = \frac{g_I \mu_0}{\hbar} \mathbf{I}, \quad (10)$$

where  $\mu_B$  and  $\mu_0$  are the Bohr and nuclear magnetons respectively, and  $g_J$ ,  $g_I$  are electrotonic and nuclear Landé factors. The action of magnetic field on the atom has two closely related effects. First, magnetic sublevels of the hyperfine levels are mixed in the magnetic field:

$$|\gamma_k m\rangle = \sum_{F_e=J_e-I}^{F_e=J_e+I} C_{kF_e}^{(e)}(B, m) |F_e, m\rangle, \quad |\eta_j \mu\rangle = \sum_{F_i=J_i-I}^{F_i=J_i+I} C_{jF_i}^{(i)}(B, \mu) |F_i, \mu\rangle, \quad (11)$$

where  $C_{kF_e}^{(e)}(B, m)$  and  $C_{jF_i}^{(i)}(B, \mu)$  are mixing coefficients depending on the field strength and magnetic quantum number ( $m$  or  $\mu$ ). The second effect is deviation of the Zeeman magnetic

sublevel splitting in the magnetic field for each hyperfine level form the linear one. It means that the additional energy of the magnetic sublevel obtained in the magnetic field is not any more linearly proportional to the field strength. In general case, new atomic states  $|\gamma_k m\rangle$  and  $|\eta_j \mu\rangle$  in the magnetic field are linear combinations of all initial hyperfine levels (4 in the case of Cs atoms in  $6^2P_{3/2}$  state and 2 in case of Cs atom in the  $6^2S_{1/2}$  state). As it is seen from Eq.(11), the hyperfine angular momentum quantum number  $F$  ceases to be a good quantum number in the magnetic field, but magnetic quantum numbers  $m$  and  $\mu$  are still good quantum numbers. This reflects the symmetry of the perturbation imposed by the magnetic field and means that only hyperfine sublevels with the same magnetic quantum numbers are mixed by the magnetic field.

The mixing coefficients  $C_{kF_e}^{(e)}(B, m)$  and  $C_{jF_i}^{(i)}(B, \mu)$  of the hyperfine states in the magnetic field and energies of these levels  ${}^{\gamma_k}E_m$ ,  ${}^{\eta_j}E_\mu$  can be found as eigenvectors and eigenvalues of the Hamilton matrix (9). In Fig.7, the energy levels obtained by the Hamilton matrix diagonalization for Cs atom in the excited  $6^2P_{3/2}$  state in the magnetic field are presented.

For Cs atoms in the ground state hyperfine level, the splitting exceeds 9 GHz, which is large in comparison to the magnetic sublevel energies obtained in the magnetic field. As a result, ground state energy levels in the magnetic field can with very good approximation be represented by the linear Zeeman effect. Namely  ${}^{\eta_j}E_\mu = g_{\eta_j} \mu_B B \mu / \hbar$ , where  $g_{\eta_j}$  is the Landé factor of the respective hyperfine level. For very weakly mixed levels they still can be represented with the hyperfine quantum number  $F_g$ . For Cs atoms in  $6^2S_{1/2}$  state we have  $g_{\eta_j} = -1/4$  for  $F_g = 3$ , and  $g_{\eta_j} = 1/4$  for  $F_g = 4$ . In the case of mixing of only two hyperfine levels, an analytical formula can be derived for mixing coefficients and for level energies in the magnetic field, similar to Breit Rabi formula, see for example [18].

The excited state density matrix created by the laser light in the magnetic field can be written as (see for example [2])

$${}^{kl}f_{mm'} = \frac{\tilde{\Gamma}_p}{\Gamma + i {}^{kl}\Delta\omega_{mm'}} \sum_{j\mu} \langle \gamma_k m | \hat{\mathbf{E}}_{exc}^* \cdot \hat{\mathbf{D}} | \eta_j \mu \rangle \langle \gamma_l m' | \hat{\mathbf{E}}_{exc}^* \cdot \hat{\mathbf{D}} | \eta_j \mu \rangle^*. \quad (12)$$

${}^{kl}\Delta\omega_{mm'} = ({}^{\gamma_k}E_m - {}^{\gamma_l}E_{m'})/\hbar$  is the energy splitting of the magnetic sublevels  $m$  and  $m'$

belonging to the excited state levels  $k$  and  $l$ . Magnetic quantum numbers of the ground state level  $\eta_j$  are denoted by  $\mu$  and magnetic quantum numbers of the excited state level  $\gamma_{k,l}$  by  $m$  and  $m'$ . In this last expression it is assumed that two magnetic sublevels of the excited state, that initially belonged to two different hyperfine levels, can have the same energy and can be excited simultaneously and coherently at some specific magnetic field strength. This means that nonzero field level crossing signals [2] are included in this model. At the same time, for practical calculations performed in this work this is of no relevance, since no nonzero magnetic field level crossings take place at the values  $B \leq 55$  Gauss used in the experiment.

In our particular simulation, we assume that when we scan the laser frequency in the manifold of splitted in the external magnetic field magnetic sublevels, only those transitions that are in an exact resonance with the laser field are excited. So at each radiation frequency, a specific for this frequency density matrix is calculated. Of course, density matrix is dependent also on the magnetic field strength, which determines magnetic sublevel splitting and wave function mixing and as a result, transition probabilities between magnetic sublevels.

In general case, the intensity of the fluorescence with a specific polarization  $\mathbf{E}_{obs}$  in a transition between excited  $\gamma_k$  and final  $\eta_j$  state in the magnetic field can be calculated according to [2]:

$$I(\mathbf{E}_f) = I_0 \sum_{mm'\mu} \sum_{klj} \langle \gamma_k m | \hat{\mathbf{E}}_{obs}^* \cdot \hat{\mathbf{D}} | \eta_j \mu \rangle \langle \gamma_l m' | \hat{\mathbf{E}}_{obs}^* \cdot \hat{\mathbf{D}} | \eta_j \mu \rangle^{*kl} f_{mm'}. \quad (13)$$

Final state of the transition may or may not coincide with the atomic ground state from which the absorption started. In lower row graphs of Fig.6*a,b*, the fluorescence spectra (line positions and relative intensities) are shown as vertical bars, for the case of excitation from  $F_g = 4$  (*a*) and  $F_g = 3$  (*b*), with linear and circular light polarizations. The dashed lines again show the resulting spectra supposing that each component has a Lorentz shape line with 55 MHz width. The results for  $B = 55$  Gauss in Fig.6 represent graphical illustration of the calculation approach for the case of elementary polarizations ( $\pi$ ,  $B = B_x$ , and  $\sigma^+$ ,  $B = B_z$ ). For other geometrical configurations, the situation is more complex to be presented by

vertical bars, since two or even three elementary polarization components may be involved.

This approach to calculate spectra in the magnetic field and in the absence of the field was used in the simulation of experimentally observed signals. The simulation was done for all the experimentally recorded spectra shown in Figs.3-5, the results are presented by solid lines. One can see rather good agreement between the theoretical and experimental results. Some discrepancy observable in the graphs may be attributed to the following factors. First, the simulation model implies Lorentz profile, rather than Voigt one, for individual transitions, and this simplification may introduce some spectral distortions. Second, the cell geometry (narrow gap between the thick windows) imposes additional (polarization sensitive) asymmetry on the spatial distribution of the emission. The fluorescence emitted under noticeable range of angles around  $90^\circ$  may be guided towards the photodiode by [multiple] grazing reflections from the external/internal faces of the window. Third, the recorded spectra may be affected by anisotropic elastic collisions of polarized atoms with the cell walls.

#### IV. CONCLUSION

The resonance fluorescence of Cs vapor layer of sub-micron thickness has been studied in the presence of moderate ( $\sim 50$  Gauss) external magnetic field, under excitation of atoms by the laser radiation tuned to the frequency region of D2 line. The spectra recorded for various reciprocal orientations of magnetic field and laser polarization (linear, circular) exhibit substantial frequency shift, modification of peak amplitude and line shape for individual hyperfine transitions. These changes originate from mixing of the hyperfine levels of the upper state  $6^2P_{3/2}$  and become observable because of intrinsic sub-Doppler nature of atomic signal in an extremely thin cell. The simulation has been performed by means of a quantum density matrix in the broad line approximation for a weak absorption regime, taking into account mixing of magnetic sublevels of the hyperfine levels and their non-linear shift in magnetic field. The results of simulation show good agreement with the experimental

results, which indicates that other possible effects (anisotropy in long-range atom-surface interaction, coherent and propagation effects, etc.) have no practical contribution in the conditions of our study.

Zeeman splitting of hyperfine sublevels in vapor media for moderate magnetic field has been observed in selective reflection [4] and saturated absorption [19] spectroscopy. Nevertheless, direct recording of fluorescence (and possibly absorption) spectra using extremely thin cells is a more straightforward method, since the signal in this case is not influenced by contribution from other unavoidable processes (dispersion and non-linear effects, crossover resonances, etc.). Sub-Doppler resolution that is a necessary condition for observation of Zeeman splitting is satisfied also for atomic beams, as well as for cold atoms. In these cases, however, cumbersome optical setups are required. Moreover, application of a magnetic field may perturb initial properties of atomic system (the case of cold atoms in magneto-optical traps).

The results of present work can be used for high spatial resolution magnetometry. Indeed, the interaction of laser radiation with atomic system responsible for magnetic sensitivity takes place in the sub-micron gap between the cell windows. Note that also the transverse dimensions of the interaction region can be essentially reduced (to the micrometer range) by means of focussing the laser beam. Extremely small sensor size of corresponding magnetometer device may allow the fine mapping of magnetic field spatial distribution that can be important for many applications, in particular for testing high-gradient magnetic fields. The magnetic field sensitivity can be noticeably enhanced by use of Rb D2 line where the smaller splitting of the upper state ( $5^2P_{3/2}$ ) will cause recordable level mixing effects at much lower  $B$ - fields ( $\sim 1$  Gauss). It should be noted that though suggested device will have much lower sensitivity than other optical magnetometer schemes (in particular, ones based on nonlinear Faraday and Hanle effects), there are several advantages that justify its possible application, namely: i) unique spatial resolution, ii) simplicity of optical setup, iii) extended upper limit of measured  $B$ - fields.

**Acknowledgments.** This work was supported, in part, by grants #00-378 and #00-381 of the Ministry of Economics of Armenia, as well as by ANSEF grant No. PS18-01. The authors are grateful to A. Sarkisyan for his valuable contribution to fabrication of the ETC, and to Yu. Malakyan for stimulating discussions.

## REFERENCES

- [1] P. Tremblay, A. Michaud, M. Levesque, S. Thériault, M. Breton, J. Beaubien, N. Cyr, Phys. Rev. A **42**, 2766 (1990)
- [2] J. Alnis, M. Auzinsh, Phys. Rev. A **63**, 023407 (2001)
- [3] A. Weis, V.A. Sautenkov, T.W. Hansch, J. Phys. II France **3**, 263 (1993)
- [4] N. Papageorgiou, A. Weis, V.A. Sautenkov, D. Bloch, M. Ducloy, Appl. Phys. B **59**, 123 (1994)
- [5] M. Auzinsh, A.V. Stolyarov, M. Tamanis, R. Ferber, J. Chem. Phys. **105**, 37 (1996)
- [6] M. Auzinsh, Physica Scripta **95**, 12 (2001)
- [7] D. Sarkisyan, D. Bloch, A. Papoyan, M. Ducloy, Opt. Commun. **200**, 201 (2001)
- [8] B. Zambon, G. Nienhuis, Opt. Commun. **143**, 308 (1997)
- [9] C.E. Theodosiou, Phys. Rev. A **30**, 2881 (1984)
- [10] M. Auzinsh, R. Ferber, *Optical Polarization of Molecules*, (Cambridge University Press, Cambridge UK, 1995)
- [11] M. Tamanis, M. Auzinsh, I. Klincare, O. Nikolayeva, A. V. Stolyarov, R. Ferber, J. Chem. Phys. **106**, 2195 (1997)
- [12] D.A. Varshalovich, A.N. Moskalev, V.K. Khersonskii, *Quantum Theory of Angular Momentum*, (World Scientific, Singapore, 1988)
- [13] I.I. Sobelman, *Atomic Spectra and Radiative Transitions*, (Springer-Verlag, Berlin, 1979)
- [14] R.N. Zare, *Angular Momentum* (J. Wiley and Sons, New York, 1988)
- [15] J. Alnis, M. Auzinsh, J. Phys. B: At. Mol. Opt. Phys. **34** (2001) 3889 – 3898.



- [16] G. Théobald, N. Dimarcq, V. Giordano, A. Hamel, P. Cèrez, J. Appl. Phys. **66**, 4581 (1989)
- [17] M. Auzinsh, Can. J. Phys. **75**, 853 (1997)
- [18] E.B. Aleksandrov, M.P. Chaika, G.I. Khvostenko, *Interference of Atomic States*, (Springer-Verlag, New York, 1993)
- [19] O. Schmidt, K.-M. Knaak, R. Wynands, D. Meschede, Appl. Phys. B **59**, 167 (1994)

## FIGURES

FIG. 1. Relevant energy levels for D2 line of Cs including hyperfine structure and relative transition probability.

FIG. 2. Geometrical configuration of the experiment. Laser radiation propagation  $\mathbf{k}$  is along  $z$  axis; arrows show various polarization cases (linear, circular left- and right-handed). Magnetic field is applied along  $x$ ,  $y$ , or  $z$  axis. Cs ETC: extremely thin (sub-micron) cell containing Cs vapor.

FIG. 3. Experimental (*scatter circles*) and theoretical (*lines*) fluorescence spectra of  $\nu_4$ :  $F_g = 4 \rightarrow F_e = (2), 3, 4, 5$  (a) and  $\nu_3$ :  $F_g = 3 \rightarrow F_e = 2, 3, 4, (5)$  (b) transitions without magnetic field (*upper row*) and with  $B_z = 55$  Gauss magnetic field (*lower row*). Incident radiation polarization: linear (*left column*), circular right-handed (*middle column*), and left-handed (*right column*). The frequency increases rightwards; the arbitrary units of the vertical (intensity) axis are the same for all the graphs.

FIG. 4. Experimental (*scatter circles*) and theoretical (*lines*) fluorescence spectra of  $\nu_4$ :  $F_g = 4 \rightarrow F_e = (2), 3, 4, 5$  (a) and  $\nu_3$ :  $F_g = 3 \rightarrow F_e = 2, 3, 4, (5)$  (b) transitions without magnetic field (*upper row*) and with  $B_x = 55$  Gauss magnetic field (*lower row*). Incident radiation polarization: linear (*left column*), and circular (*right column*). The frequency increases rightwards; the arbitrary units of the vertical (intensity) axis are the same for all the graphs.

FIG. 5. Experimental (*scatter circles*) and theoretical (*lines*) fluorescence spectra of  $\nu_4$ :  $F_g = 4 \rightarrow F_e = (2), 3, 4, 5$  (a) and  $\nu_3$ :  $F_g = 3 \rightarrow F_e = 2, 3, 4, (5)$  (b) transitions without magnetic field (*upper row*) and with  $B_y = 55$  Gauss magnetic field (*lower row*). Incident radiation polarization: linear (*left column*), and circular (*right column*). The frequency increases rightwards; the arbitrary units of the vertical (intensity) axis are the same for all the graphs.

FIG. 6. Illustration of the fluorescence spectrum simulation for  $\nu_4$  (a) and  $\nu_3$  (b) transitions. *Vertical bars* show the relative strength of the individual fluorescence components ( $|F_e m\rangle \rightarrow |F_g \mu\rangle$  for  $B = 0$ , *upper row*; and  $|\gamma_k m\rangle \rightarrow |\eta_j \mu\rangle$  for  $B = 55$  Gauss, *lower row*). *Dashed lines* represent the sum of these (broadened) components.

FIG. 7. Splitting and shift of the hyperfine states of the  $6^2P_{3/2}$  level in the magnetic field.

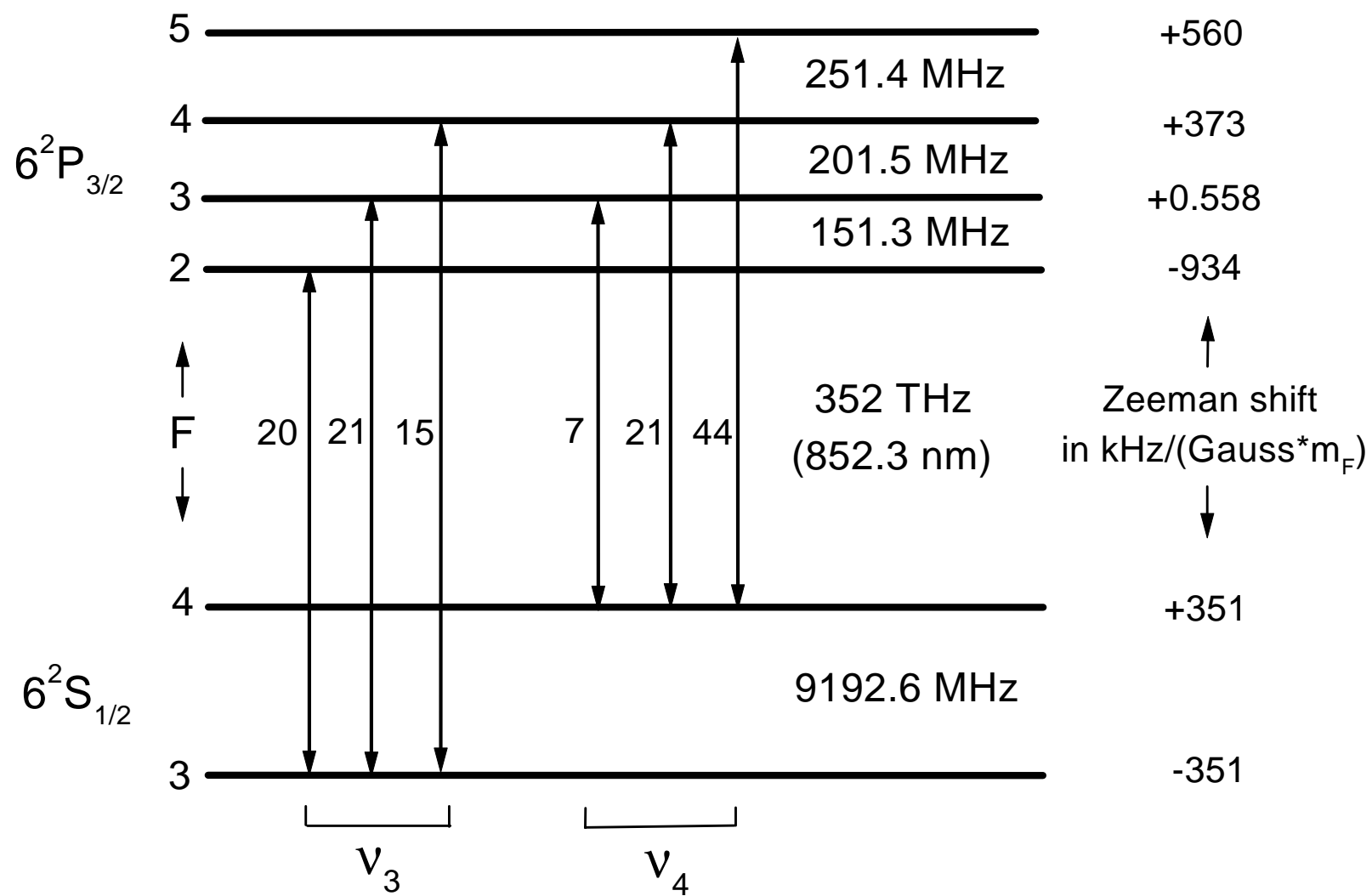


Fig. 1

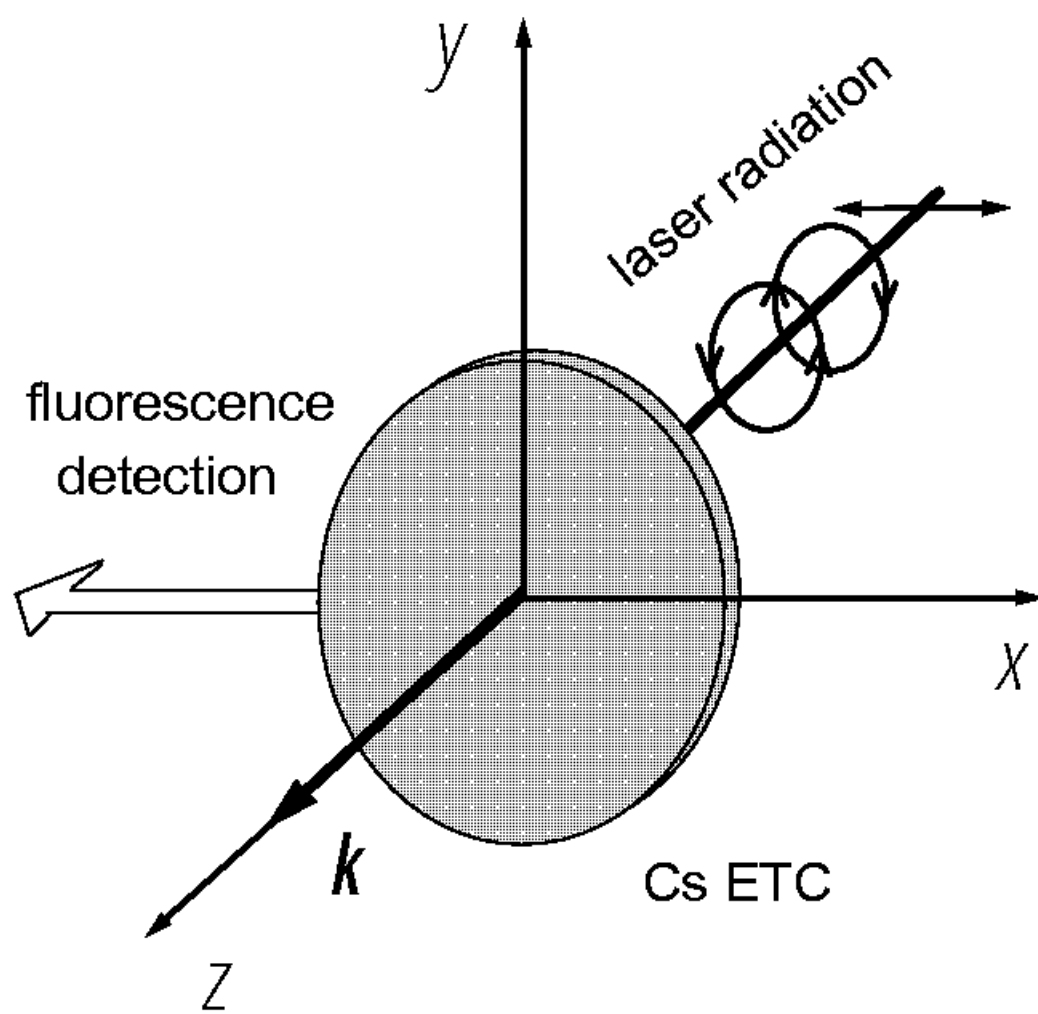


Fig. 2

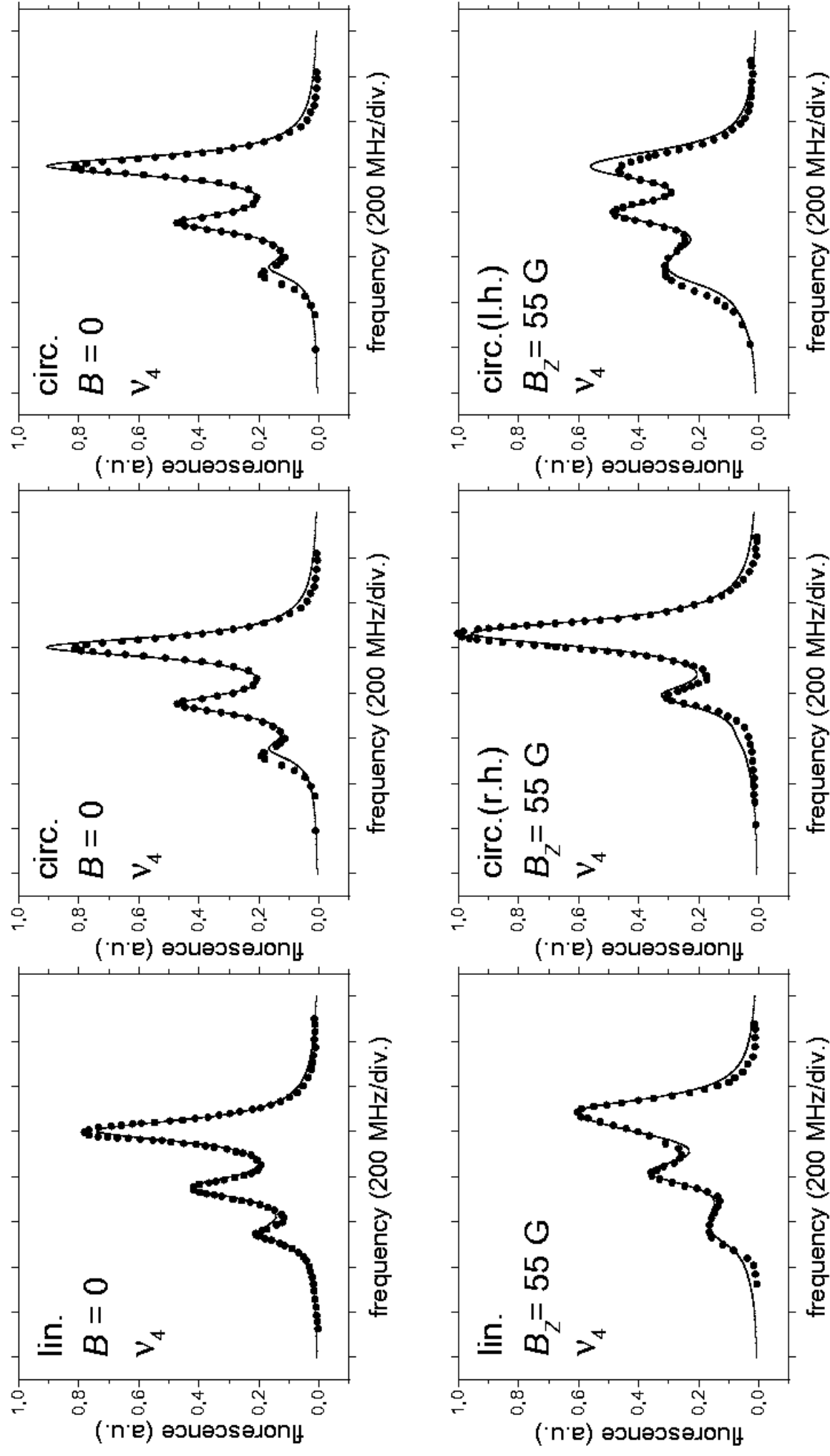


Fig. 3a

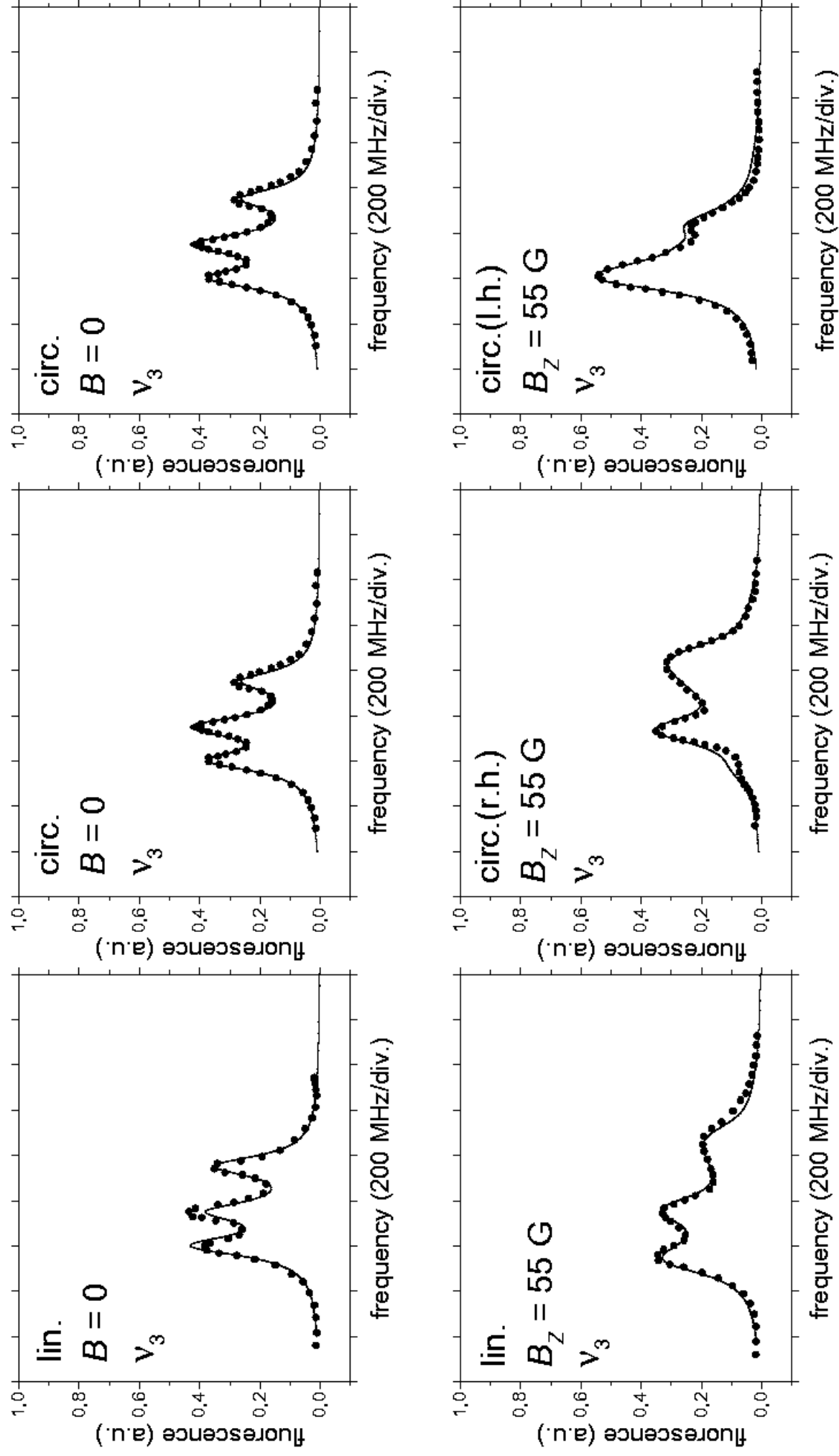


Fig. 3b

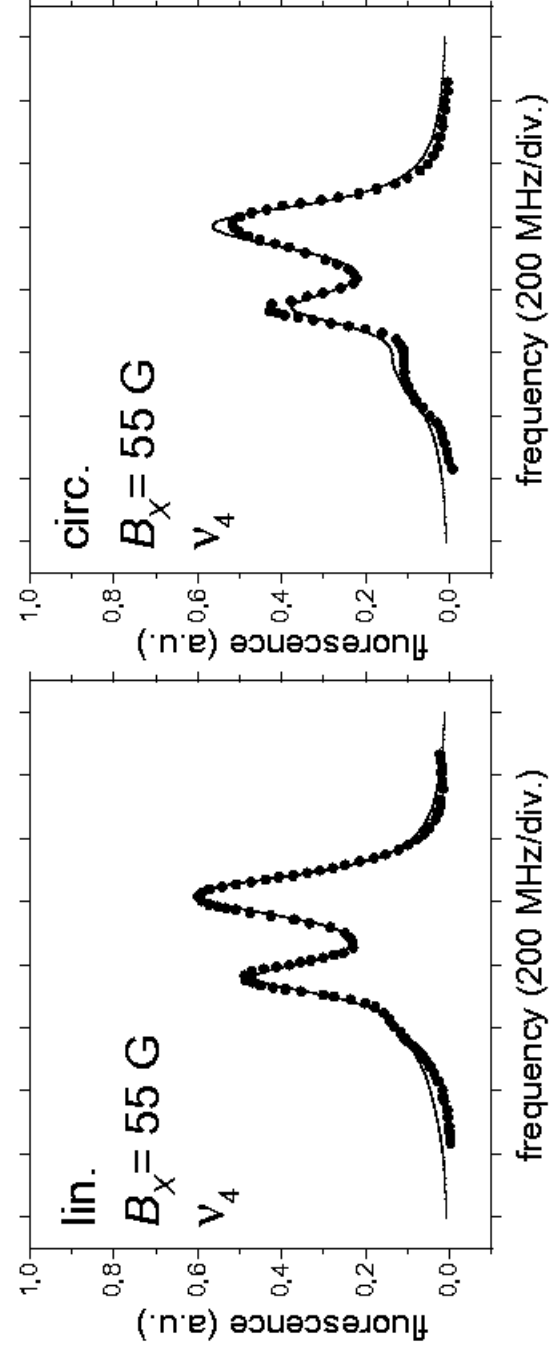
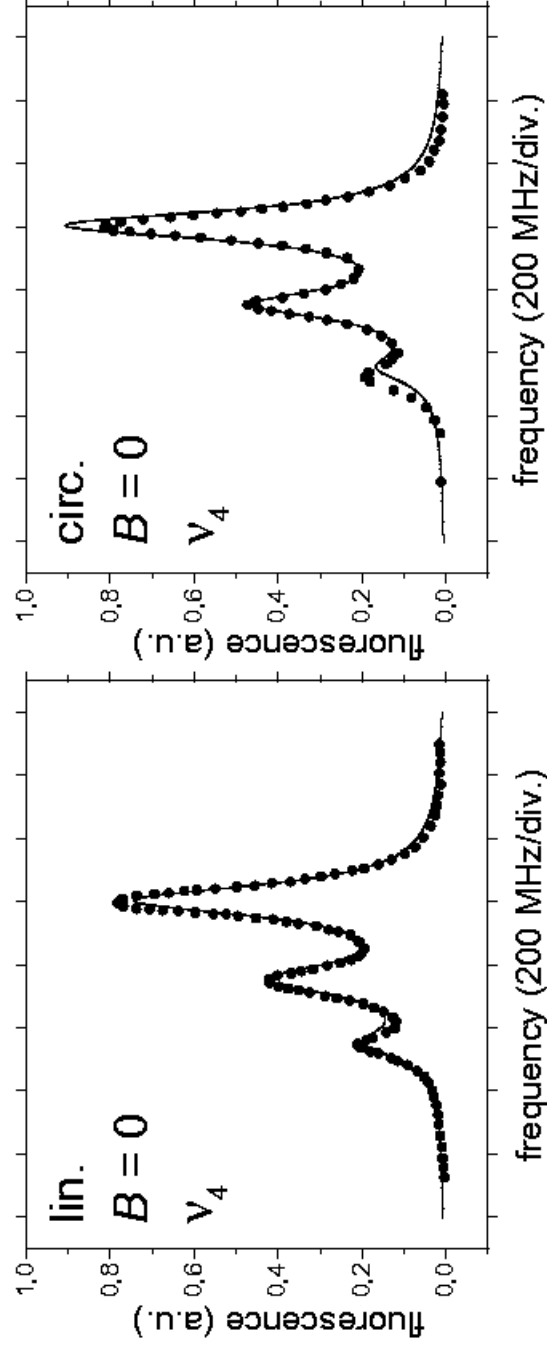


Fig. 4a



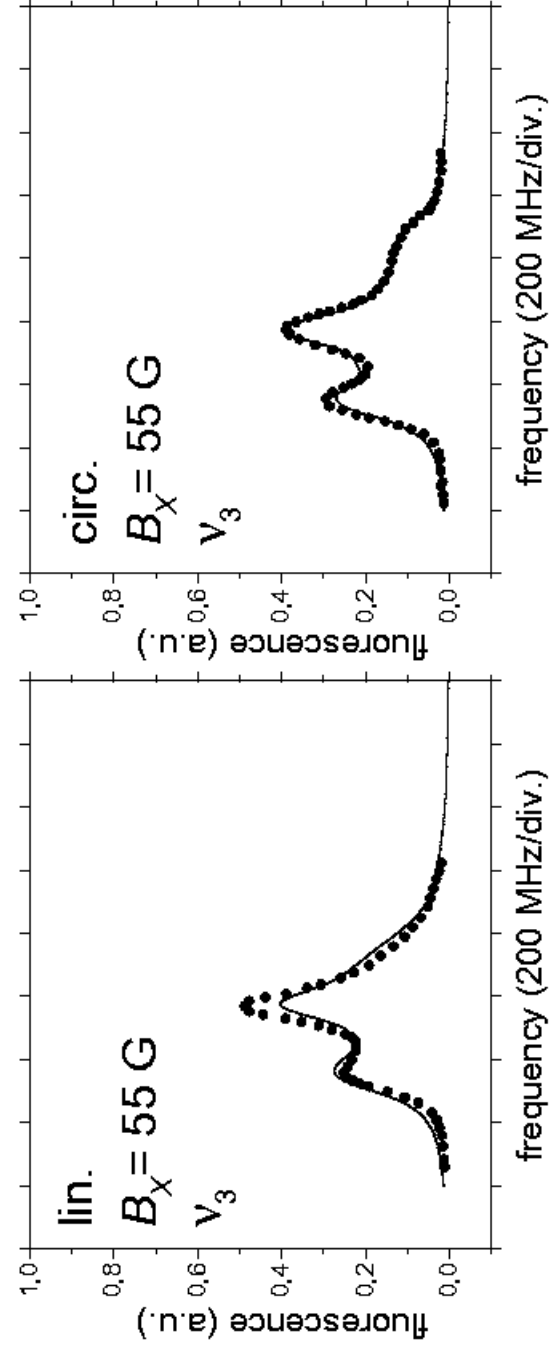
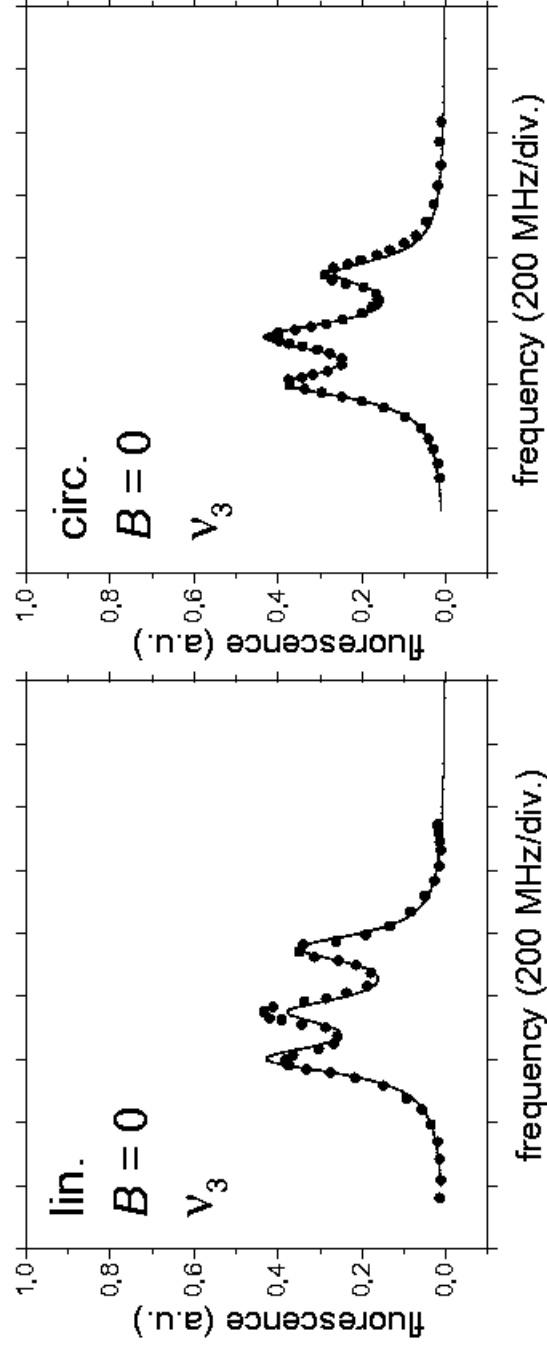


Fig. 4b

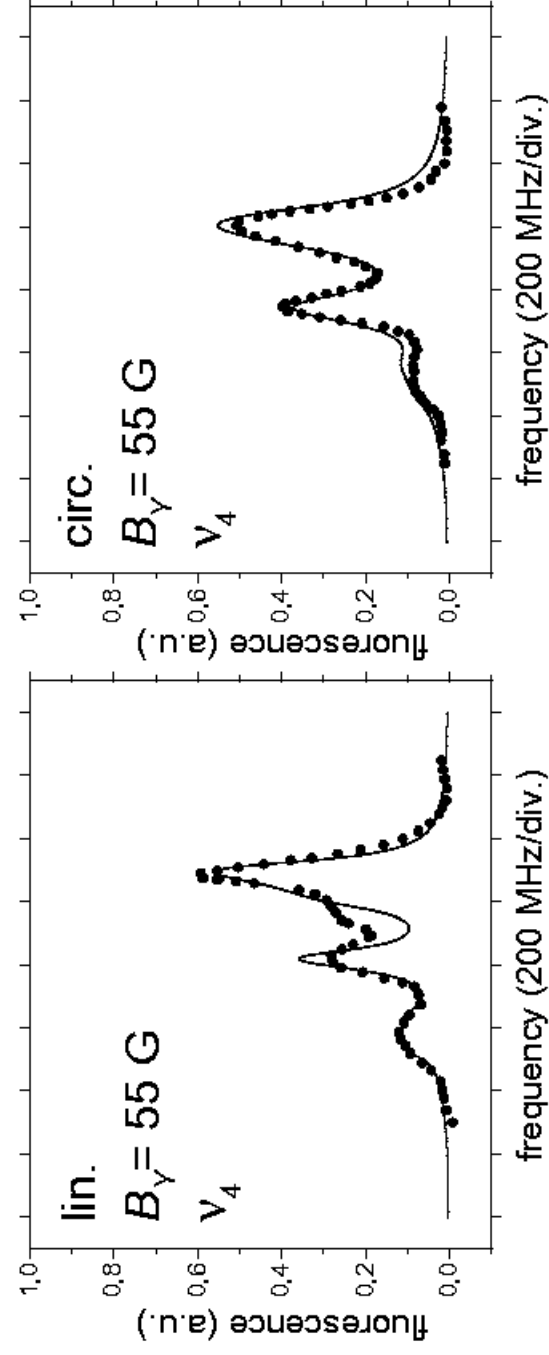
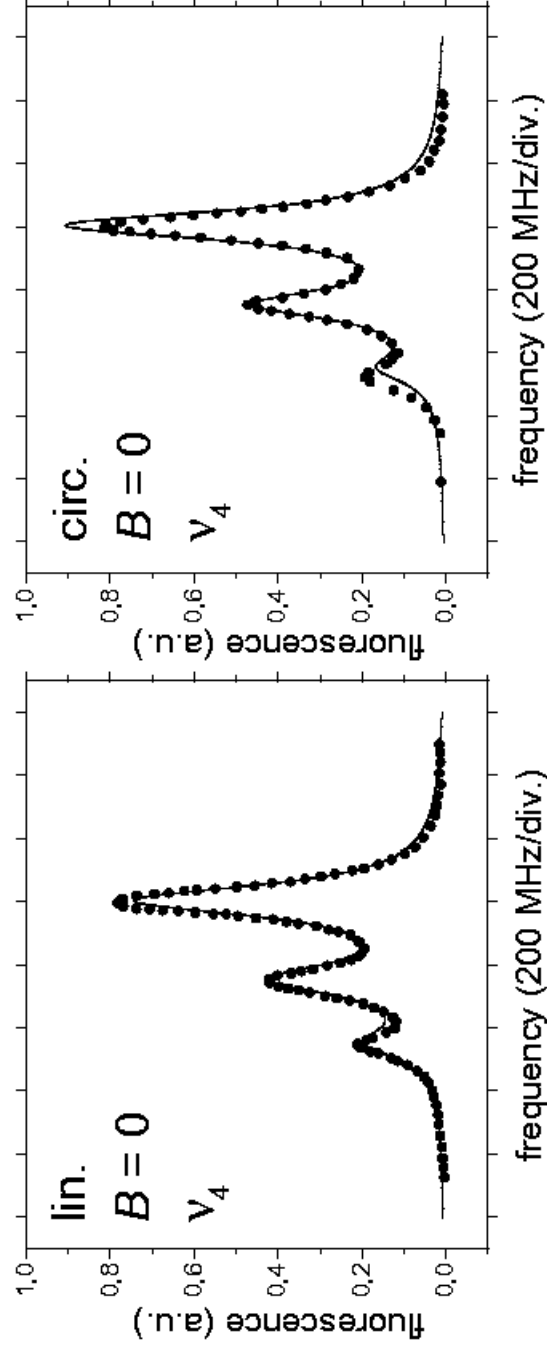


Fig. 5a

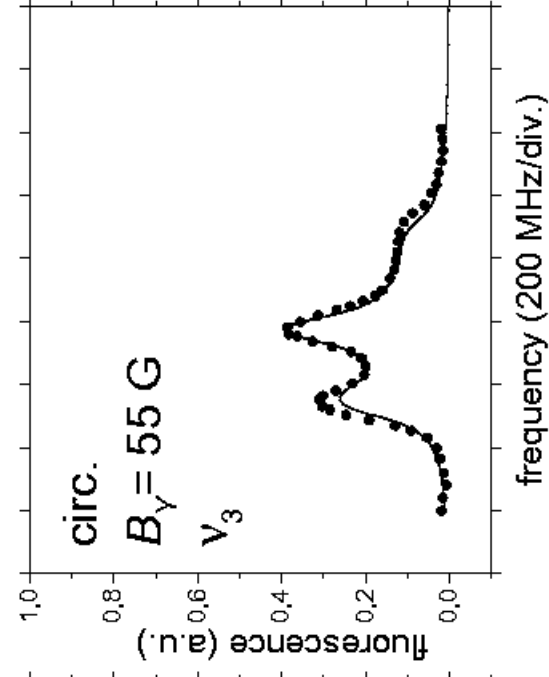
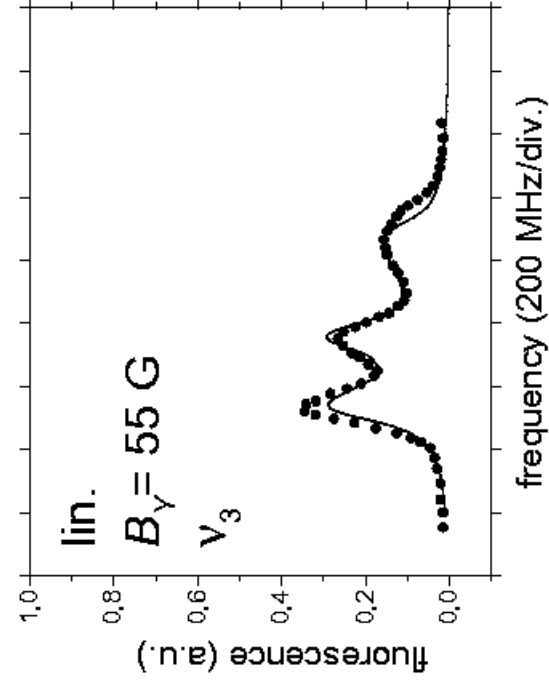
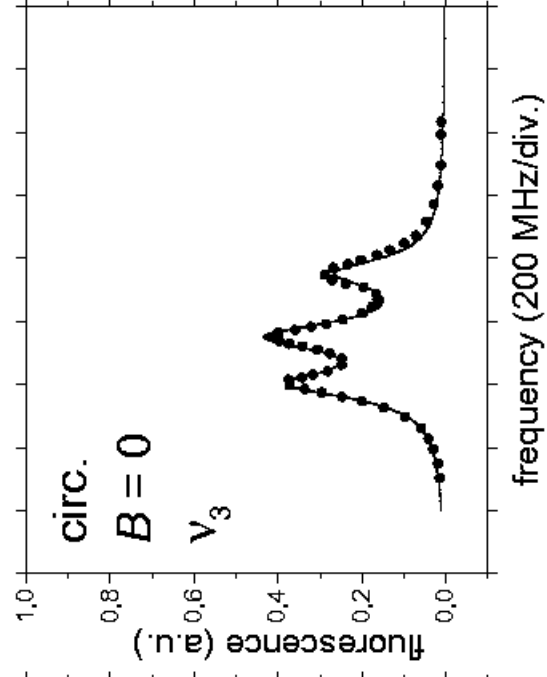
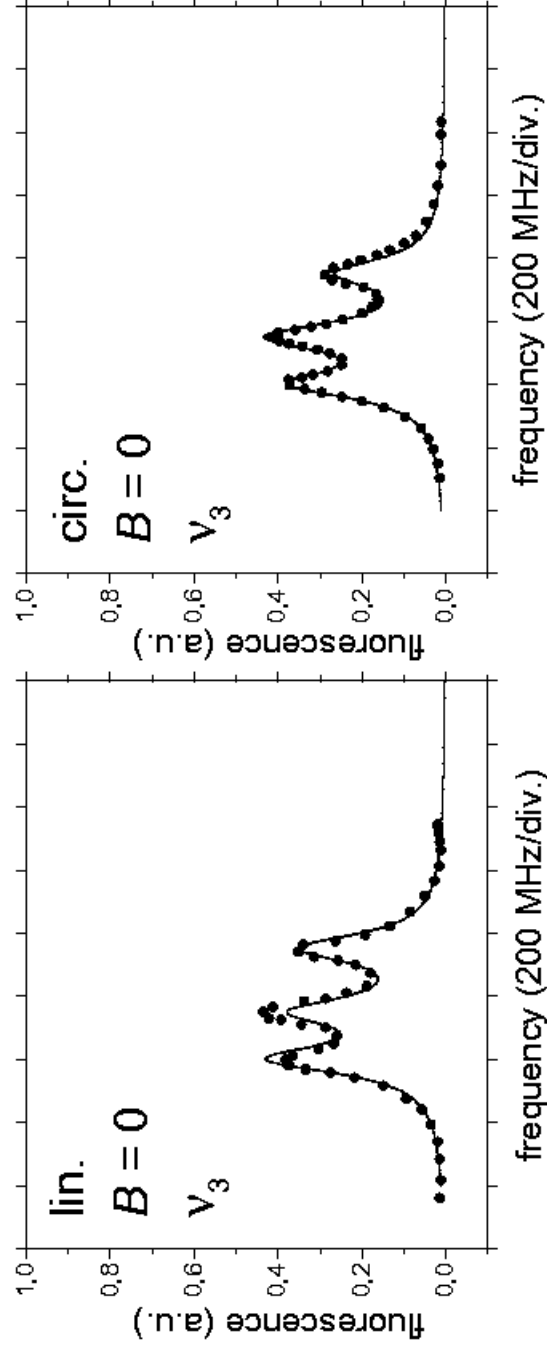


Fig. 5b

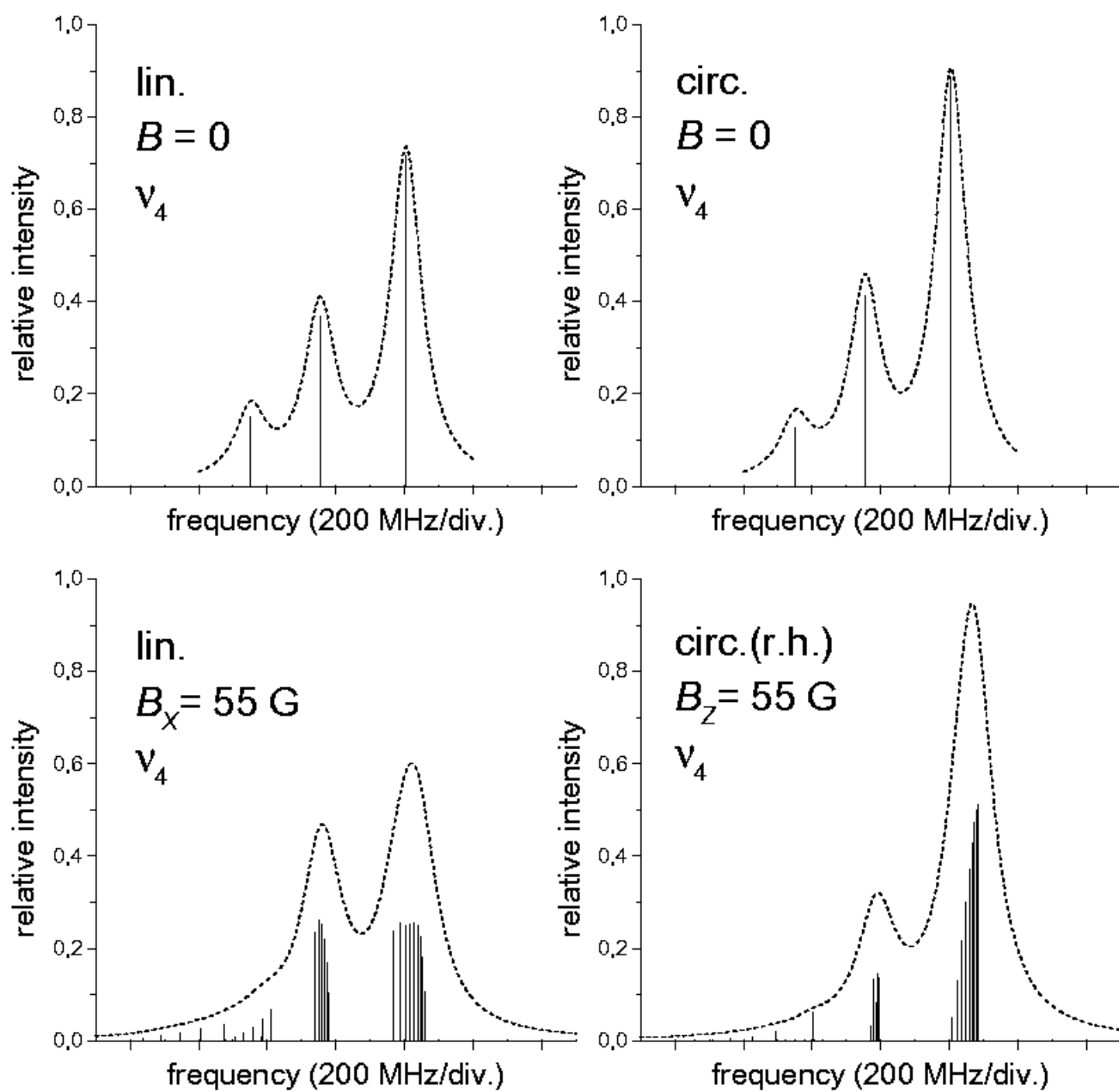


Fig. 6a

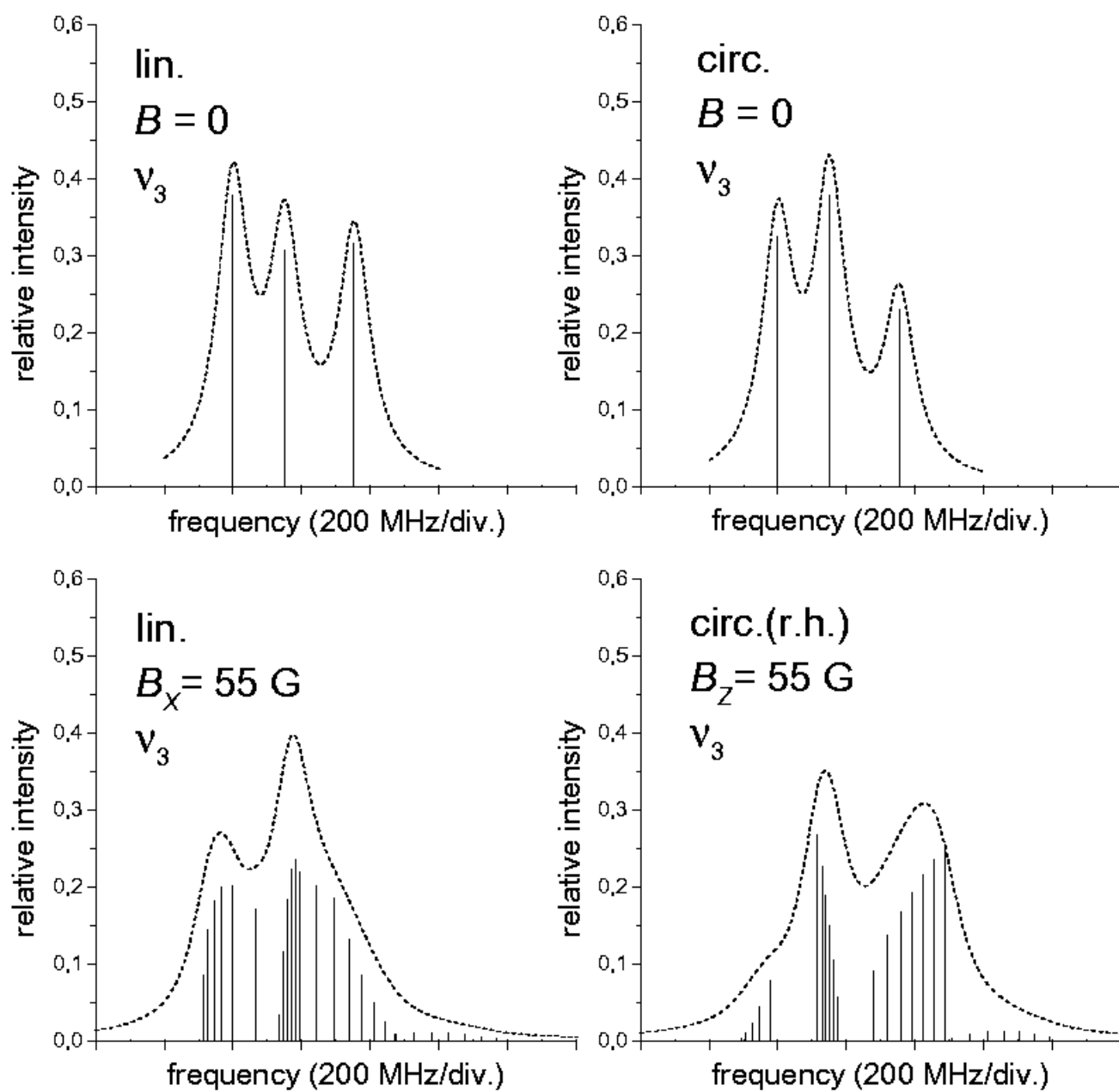


Fig. 6b

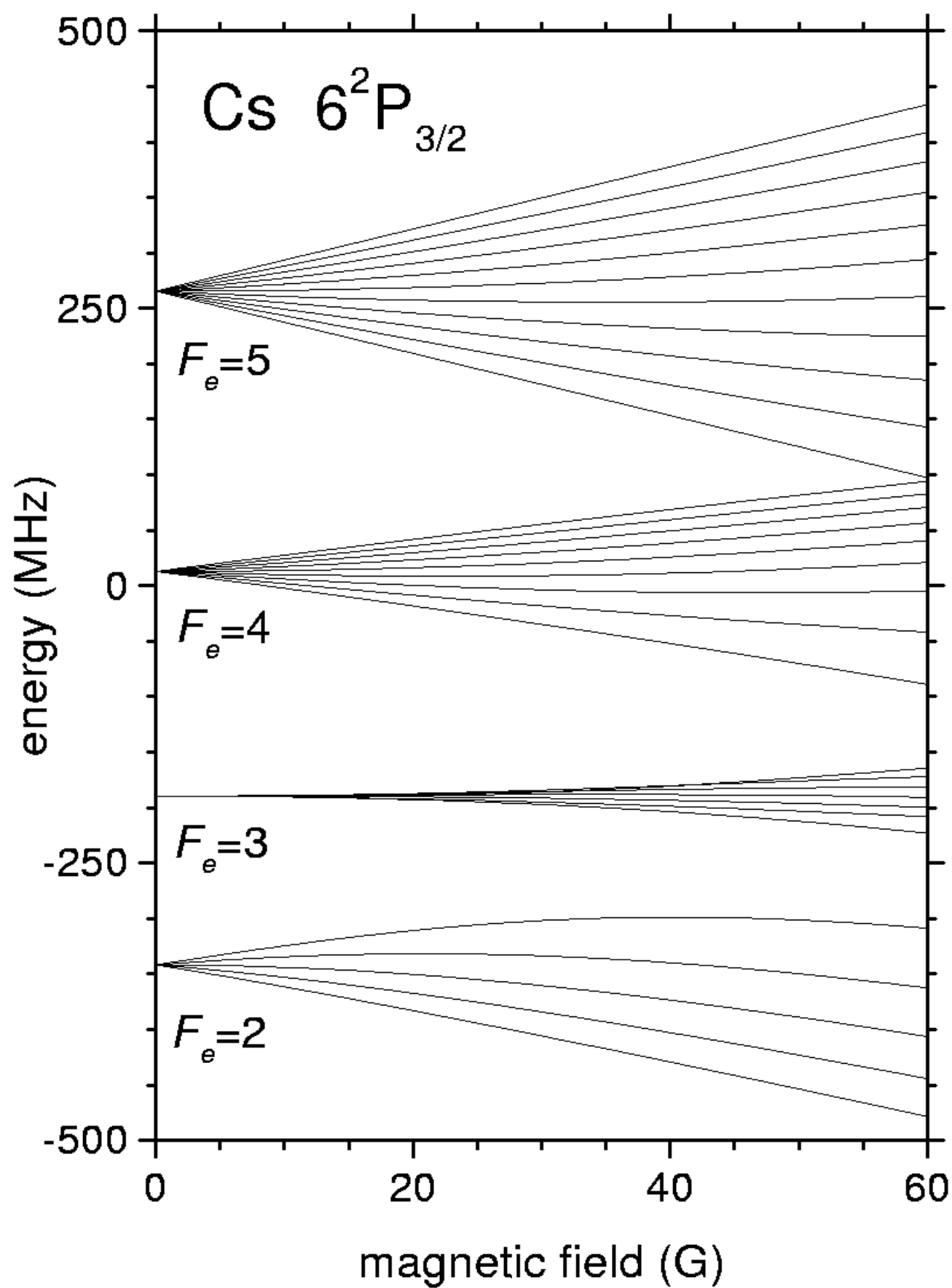


Fig. 7